Spectroscopic studies of phthalocyanines and their clusters with small molecules

J. A. Menapace and E. R. Bernstein

Citation: The Journal of Chemical Physics **87**, 6877 (1987); doi: 10.1063/1.453382
View online: http://dx.doi.org/10.1063/1.453382
View Table of Contents: http://aip.scitation.org/toc/jcp/87/12
Published by the American Institute of Physics

Spectroscopic studies of phthalocyanines and their clusters with small molecules[a)]

J. A. Menapace and E. R. Bernstein
Department of Chemistry, Condensed Matter Sciences Laboratory, Colorado State University, Fort Collins, Colorado 80523

(Received 2 April 1987; accepted 25 August 1987)

van der Waals clusters of free base phthalocyanine (H_2Pc) and magnesium phthalocyanine (MgPc) with small hydrocarbons [C_nH_{2n+2} ($n = 1,2,3$)], hydrogen bonding solvents (H_2O, MeOH, EtOH), and CO_2 are studied in the gas phase using supersonic molecular jet spectroscopy. Fluorescence excitation spectra of the cluster systems are characterized in the 0_0^0 regions of the cluster $S_1 \leftarrow S_0$ transitions. Forbidden low frequency cluster chromophore out-of-plane vibronic transitions are induced by clustering in the majority of the cluster systems studied. This low frequency motion is characterized using an out-of-plane normal coordinate analysis on the H_2Pc moiety. Calculations of the binding energy and ground state geometry for the clusters are carried out employing Lennard-Jones (6-12-1) and hydrogen bonding (10-12-1) potentials. Comparison between the calculations and experiments allow for the identification of specific configurations responsible for the cluster vibronic transitions observed. The cluster vibronic spectra and theoretical calculations suggest that stable H_2Pc and MgPc solvation sites are located over the phthalocyano core and not over peripheral ring centers. The H_2Pc/hydrocarbon cluster experimental and calculational results parallel those obtained for benzene and *N*-heterocycle/hydrocarbon clusters studied previously. The H_2Pc and MgPc/alcohol cluster spectra and calculated geometries suggest that the solvent OH group is intimately involved in the intermolecular interactions and contributes significantly to the observed spectroscopic shifts.

I. INTRODUCTION

Supersonic molecular jet spectroscopy has been extensively utilized to study weakly bound solute/solvent van der Waals (vdW) clusters in an ultracold, isolated, gas phase environment. These investigations have led to an increased understanding of the intra- and intermolecular energetics and dynamics present in the solute solvent systems as well as the nucleation and growth of small clusters.[1]

Presently, little information is available concerning the gas phase vdW clusters of macrocyclic species such as phthalocyanines[2] (Pc's) and related compounds[3] with small molecules even though the macrocycles themselves have been previously studied using supersonic molecular jet/laser spectroscopic techniques. Elucidation of the solvation properties exhibited by these systems is of considerable interest as it may prove useful in the overall understanding of the transport and storage of small molecules in biologically active species[4] and of the basic processes of photosynthesis.[5] The two previous studies of porphyrin clusters[3(e),3(f)] include free base porphine with argon and Zn octaethylporphyrin with benzene, methanol, water, acetonitrile, and pyridine. In general, the spectroscopic cluster shifts reported for these latter systems are somewhat larger than those found for the present phthalocyanine systems. A brief comparison between the two data sets is made at the end of this paper.

Supersonic molecular jet investigations can contribute to the resolution of a number of important concerns dealing with the behavior of Pc/solvent systems on the microscopic scale. Questions that can be considered are (1) what are the ground and excited state interaction energies between Pc and various solvents, (2) what are the preferential intermolecular interaction sites on the Pc moiety, (3) what are the most favorable cluster geometries, (4) what types of interactions are important in the intermolecular potential established between the solute and solvent, and (5) are changes in the chromophore symmetry/geometry induced by clustering. The answers to these questions will certainly be helpful to those employing Pc's or related systems in reactions and other chemical processes.

This paper reports the first supersonic molecular jet studies of the gas phase solvation of Pc's in a well-defined and controlled molecular environment. This report includes the spectroscopic results of free base phthalocyanine (H_2Pc) and magnesium phthalocyanine (MgPc) clustered with hydrocarbon solvents (CH_4, C_2H_6, and C_3H_8), hydrogen bonding solvents (H_2O, MeOH, EtOH), and CO_2 along with the calculated modeling of selected cluster characteristics. The spectroscopic results include the $\pi^* \leftarrow \pi$ fluorescence excitation (FE) spectra of the clusters near the Pc 0_0^0 transitions. The calculated results include the ground state geometry and the binding energy for each of the cluster systems studied. The H_2Pc cluster spectra and calculated geometries and binding energies are compared with those obtained for the MgPc clusters. Differences and similarities between the H_2Pc(MgPc) clusters and the aromatic hydrocarbon and *N*-heterocycle clusters are discussed. Specifically, trends in spectral shifts, relative solute/solvent orientations, and binding energies are noted. Finally, the results of an out-of-plane normal coordinate analysis for H_2Pc are dis-

[a)] Supported in part by grants from ONR and the Philip Morris Corporation.

cussed and compared to both Pc and cluster spectra within the first few hundred wave numbers of the origin transitions.

II. EXPERIMENTAL PROCEDURES

The majority of the apparatus used in these experiments has been previously described[6]; therefore, only a description of the equipment and procedures unique to the present studies will be discussed. A high temperature continuous supersonic nozzle fabricated to generate and analyze the H_2Pc and MgPc clusters is shown in Fig. 1. The expansion region is constructed by welding a stainless steel pinhole (Micro Engineering) A onto a 1/4 in. tube connector gland (Cajon VCR) B. The pinhole/gland is attached to the nozzle backing region C using a 1/4 in. tube connector (Cajon VCR) D. Stainless steel gaskets are used to insure proper connector sealing throughout the nozzle operating temperature range. This setup allows different size pinhole assemblies (nozzle throats) to be attached to the nozzle to obtain various peak experimental backing pressure and gas throughput conditions. A 100 μ pinhole is used to perform the expansion in the H_2Pc and MgPc cluster experiments. The nozzle backing region is constructed from 1/2 in. stainless steel tubing. The tubing extends through the vacuum chamber wall E passing through a vacuum quick disconnect (MDC Vacuum) F. Connection of the nozzle to the expansion gas line is accomplished using a stainless steel tube connector (Swagelok) G. Solid samples are placed in the nozzle backing region using a quartz "boat" H which can be inserted into the nozzle through the expansion gas line connection. The boat facilitates access to the nozzle backing region while the nozzle is in the vacuum chamber and is heated. It allows for easy inspection of the sample during and after an experiment without nozzle removal or nozzle cooling. The nozzle is heated using two heating coils (ARL Industries) I located around the expansion and backing regions. The heaters are capable of maintaining the nozzle at temperatures up to 650 °C. The heaters are independently controlled using two transformer assemblies. Nozzle temperature is monitored using two iron–constantan thermocouples (Omega) J placed around the expansion and backing regions. The nozzle/heater assembly is enclosed in a stainless steel shield K to minimize heat loss and to maintain uniform nozzle heating.

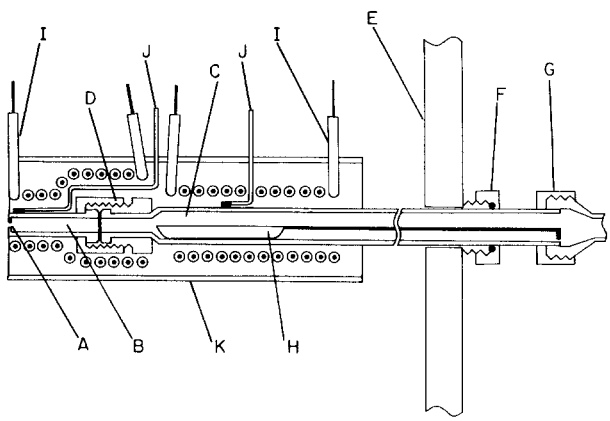

FIG. 1. High temperature continuous supersonic molecular jet nozzle (see the text).

FE spectra of the H_2Pc, MgPc, and their respective solvent clusters are obtained using a Nd^{+3}/YAG pumped DCM (Exciton) dye laser. Dye laser output is 46–60 mJ/pulse in the vicinity of the H_2Pc and MgPc 0_0^0 transitions. Total excited state fluorescence is collected using a $f/1.2$ 5 cm lens focused at 5–8 mm in front of the nozzle throat and detected by a water cooled RCA C31034 photomultiplier tube. The photomultiplier tube output is amplified 10× using an Ortec 9301 amplifier. The signal is then sent to a boxcar/computer for averaging and digital storage. Fluorescence wavelength calibration is provided by an optogalvanic cell with iron and neon lines as standards.

H_2Pc (Aldrich) and MgPc (Eastman Kodak) are purified by vacuum sublimation before use. The solid samples are pelletized prior to insertion into the nozzle to minimize and control sample consumption. Granular samples placed in the nozzle are consumed at a rate of ~45 mg/h. Pelletization reduces sample consumption by about a factor of 30 without significant loss in fluorescence intensity.

The H_2Pc and MgPc solid samples are heated to 380–640 °C to provide sufficient vapor density to perform the spectroscopy. Methane, ethane, propane, or carbon dioxide is doped into helium carrier gas at concentrations of up to 1% (partial pressure). The gas is then mixed with the H_2Pc or MgPc in the nozzle backing region and expanded using pressures ranging from 100–200 psig. Water, methanol, or ethanol is seeded into the helium carrier gas by passing the carrier gas through an in-line trap containing the liquid solvent.

Over the temperature ranges utilized in the studies, neither the H_2Pc or MgPc samples showed any visual evidence of thermal decomposition in the presence of the seeded solvent species. Additionally spectra of isolated H_2Pc and MgPc taken before and after seeding the jet with solvent are identical: no evidence is found for sample decomposition in the nozzle chamber.

Calculations of the ground state cluster binding energies and geometries are conducted using an empirical intermolecular potential generated from additive atom–atom potentials set into a Lennard-Jones format. The potential includes general nonbonding (6-12), monopole charge (1), and hydrogen bonding (10-12) terms.[7] This potential has been successfully applied in our previous work on benzene and *N*-heterocycle/solvent systems.[8] The calculations are consistent with experimental observations with regard to cluster binding energy, the number of distinct cluster configurations observed, and the intermolecular vibronic structure present in the spectra. The H_2Pc and MgPc structures used in the calculations are obtained from crystal structure data.[9] The atom–atom potential for magnesium is approximated using experimentally determined polarizabilities,[10] interatomic distance,[11] and the Slater–Kirkwood approximation.[12] Atomic partial charges employed to model the monopole charge interaction are taken from extended Hückel[13] calculations. The hydrocarbon and water structures are those previously used in studying benzene and *N*-heterocycle clusters.[1(f),1(g),8] The CO_2, MeOH, and EtOH structures are

TABLE I. Calculated out-of-plane mode frequencies for H_2Pc.

Calculated mode energy (cm^{-1})	D_{2h} symmetry species	Observed overtone[a] energy (cm^{-1})	Mode designation
14.8	B_{1u}	31.2(15.6)	*A*
24.5	B_{1u}	51.8(25.9)	*B*
84.0	B_{1u}	163.7(81.9)	*C*
33.1	A_u	71.4(35.7)	*D*
71.7	A_u	141.7(70.9)	*E*
38.6	B_{2g}	85.4(42.7) or 100.6(50.3)	*F*
72.1	B_{2g}	176(88) or 203.1(101.6)	*G*
38.2	B_{3g}	85.4(42.7) or 100.6(50.3)	*H*
71.4	B_{3g}	176(88) or 203.1(101.6)	*J*

[a] Values in parentheses are forbidden fundamental mode energies inferred from overtone transitions.

taken from Refs. 14, 15, and 16, respectively.

The out-of-plane normal coordinate analysis for H_2Pc is conducted using the FG matrix method of Wilson *et al.*[17] The details of the analysis will be reported elsewhere.[18] Briefly, the nuclear motion is modeled using a set of 82 internal coordinates; 48 C–C(N) bond torsions, 18 C(N)–H bond wags, and 16 C–C(N) bond wags. The valence force field for the *F* matrix consists of the diagonal force constants describing the out-of-plane ground state motions in benzene.[19] In this gross approximation, all H_2Pc bond torsion force constants are assumed to be the same as the C–C torsions in benzene. All bond wag force constants are assumed to be the same as the benzene C–H wags. The out-of-plane vibrations calculated using these assumptions should give a reasonable estimate of the large amplitude low frequency motion ($< 100\ cm^{-1}$) observed in the spectrum as these modes are, for the most part, insensitive to minor changes in the force constants governing the motion. For example, varying the force constants by $\pm$ 10% causes the lowest frequency mode calculated at 14.8 cm^{-1} to shift by about $\pm 0.8\ cm^{-1}$. The high frequency motion ($\cong 500\ cm^{-1}$) calculated using these assumptions are, on the other hand, sensitive to changes in the force constants. These modes, however, have no bearing in the present study so they need not be discussed. The secular equation describing the nuclear motion is symmetry factored into four species sets (B_{1u}, A_u, B_{2g}, and B_{3g}) under the D_{2h} point group. The factored equations are individually diagonalized to yield 15 B_{1u}, 13 A_u, 13 B_{2g}, and 14 B_{3g} out-of-plane frequency eigenvalues and eigenvector normal modes. (See Table I.)

TABLE II. Observed vibronic transitions in the vicinity of the H_2Pc 0_0^0.

Energy (vac. cm^{-1})	Wavelength (vac. Å)	Energy relative to 0_0^0 (cm^{-1})	Assignment[a]
15 131.8	6608.6	0	0_0^0
15 163.0	6595.0	31.2	A_0^2
15 183.6	6586.1	51.8	B_0^2
15 193.9	6581.6	62.0	A_0^4
15 203.2	6577.6	71.4	D_0^2
15 215.6	6572.2	83.8	$A_0^2 + B_0^2$
15 217.2	6571.5	85.4	F_0^2 or H_0^2
15 225.8	6567.8	93.9	b
15 228.0	6566.9	96.2	$A_0^1 + C_0^1$
15 232.4	6564.9	100.6	F_0^2 or H_0^2
15 258.7	6553.6	126.9	b
15 273.5	6547.3	141.7	E_0^2
15 290.5	6540.0	158.7	$126.9 + A_0^2$
15 295.5	6537.9	163.7	C_0^2
15 307.8	6532.6	176	G_0^2 or J_0^2

[a] Assignments based on normal coordinate analysis results (see Table I).
[b] Modes possibly due to in-plane motion.

III. RESULTS

A. Isolated ultracold molecular FE spectra of H_2Pc and MgPc

Figure 2 presents the FE spectrum of the H_2Pc $S_1 \leftarrow S_0$ transition (Q_x band) in the vicinity of the 0_0^0. The spectrum is taken at 200 psig helium backing pressure (P_0), a nozzle expansion region temperature (T_e) of 570 °C, and a nozzle backing region temperature (T_b) of 460 °C. The general nature of the spectrum has been previously described.[2] The purpose of its reproduction in this paper is (1) to present a detailed account of the low frequency vibronic transitions observed in the vicinity of the 0_0^0 which have not been previously reported in the literature, Table II, and (2) to provide an isolated chromophore spectrum which can be compared to the cluster spectra, all of which are taken under

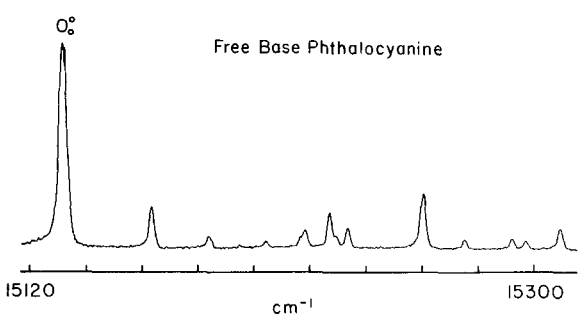

FIG. 2. FE spectrum of 0_0^0 region of H_2Pc taken at $T_e = 570$ °C, $T_b = 460$ °C, and $P_0 = 200$ psig He. Peak assignments are given in Table II.

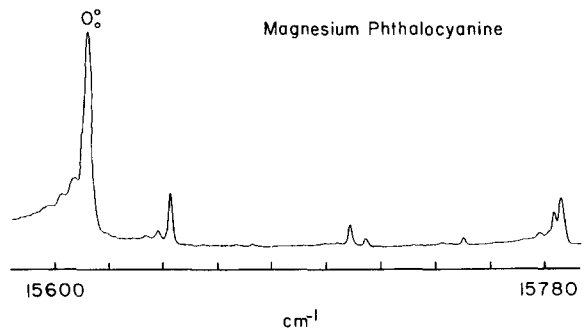

FIG. 3. FE spectrum of 0_0^0 region of MgPc taken at $T_e = 630$ °C, $T_b = 397$ °C, and $P_0 = 120$ psig He. Peak assignments are given in Table III.

TABLE III. Observed vibronic transitions in the vicinity of the MgPc 0_0^0.

Energy (vac. cm^{-1})	Wavelength (vac. Å)	Energy relative to 0_0^0 (cm^{-1})	Assignment[a]
15 612.1	6404.5	0	0_0^0
15 643.0	6392.6	30.9	A_0^2
15 666.7	6383.0	54.6	B_0^2
15 673.2	6380.3	61.1	A_0^4
15 704.4	6367.6	92.3	F_0^2 or H_0^2
15 709.0	6365.8	96.9	b
15 714.6	6363.5	102.5	F_0^2 or H_0^2
15 742.1	6352.4	130.0	
15 750.1	6349.2	138.0	E_0^2
15 778.0	6337.9	165.9	
15 783.5	6335.7	171.4	
15 786.0	6334.7	173.9	b

[a] Assignments based on normal coordinate analysis results (see Table I).
[b] Modes are due to in-plane motion.

nearly identical experimental conditions.

The FE spectrum of the MgPc $S_1 \leftarrow S_0$ transition (Q band) in the vicinity of the 0_0^0 is shown in Fig. 3. The spectrum is taken using $P_0 = 120$ psig helium, $T_e = 630$ °C, and $T_b = 397$ °C. Table III lists the energies of the vibronic transitions observed in this portion of the spectrum.

B. Hydrocarbon clusters: CH_4, C_2H_6, and C_3H_8

The H_2Pc/hydrocarbon cluster FE spectra observed in the vicinity of the H_2Pc 0_0^0 are presented in Fig. 4. The energies of the observed cluster transitions are listed in Table IV. In these experiments, solvent concentration is varied between 0.07% and 1% and the backing pressure is varied between 0 and 300 psig. Below 0.07% solvent concentration,

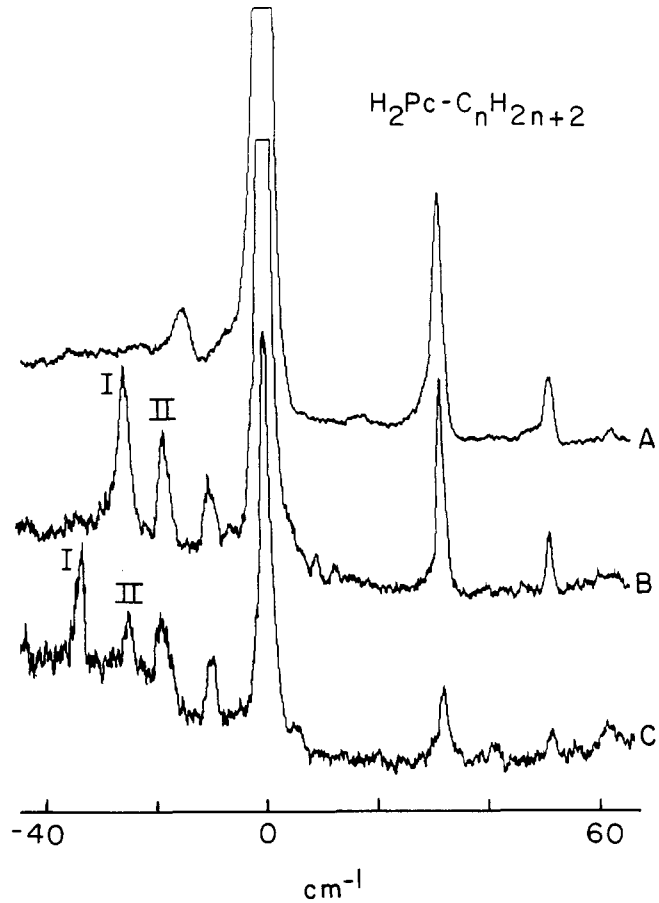

FIG. 4. FE spectra of H_2Pc/C_nH_{2n+2} clusters in the vicinity of the H_2Pc 0_0^0. The $H_2Pc(CH_4)_1$ spectrum (A) is taken at $T_e = 540$ °C, $T_b = 430$ °C, $P_0 = 200$ psig He, and 0.1% CH_4. The $H_2Pc(C_2H_6)_1$ spectrum (B) is taken at $T_e = 540$ °C, $T_b = 430$ °C, $P_0 = 160$ psig He, and 0.1% C_2H_6. The $H_2Pc(C_3H_8)_1$ spectrum (C) is taken at $T_e = 580$ °C, $T_b = 435$ °C. $P_0 = 160$ psig He, and 0.1% C_3H_8. Peak assignments are given in Table IV.

TABLE IV. H_2Pc hydrocarbon cluster transitions in the vicinity of H_2Pc 0_0^0.

Species	Energy (vac. cm^{-1})	Cluster 0_0^0 relative to H_2Pc 0_0^0 (cm^{-1})	Energy relative to cluster 0_0^0 (cm^{-1})	Assignment
$H_2Pc(CH_4)_1$	15 117.2	−14.6	0	0_0^0
	15 148.5		31.3	A_0^2
	15 163.5		51.3	B_0^2
$H_2Pc(C_2H_6)_1$	15 105.9	−25.9	0	I 0_0^0
	15 121.5		15.6	A_0^1
	15 138.6		32.7	A_0^2
	15 113.0	−18.8	0	II 0_0^0
	15 144.3		31.3	A_0^2
$H_2Pc(C_3H_8)_1$	15 098.4	−33.4	0	I 0_0^0
	15 113.2		14.8	A_0^1
	15 106.7	−25.1	0	II 0_0^0
	15 122.4		15.7	A_0^1
	15 138.1		31.4	A_0^2

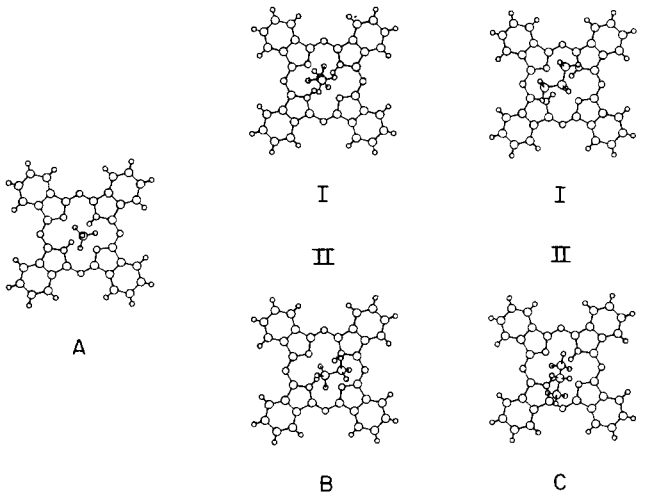

FIG. 5. Calculated minimum energy geometries for $H_2Pc(CH_4)_1$ (A), $H_2Pc(C_2H_6)_1$ (B), and $H_2Pc(C_3H_8)_1$ (C). The cluster binding energies and solute/solvent center-of-mass coordinates are given in Table V.

no cluster transitions are observed; above about 0.3%, the cluster spectra appear broad and featureless to the red of the H_2Pc 0_0^0. Below 50 psig backing pressure, the spectra become broad; at 100 to 300 psig, no new cluster transitions emerge in the region probed.

Sharp spectra of MgPc/hydrocarbon clusters could not be generated through the range of 0.06% to 3% solvent concentration, the spectra vary from no observable cluster transitions to broad cluster bands which extend some 60 cm^{-1} to the red of the MgPc origin. The exact reason for this behavior is not clear. The MgPc sample, however, is not decomposed by the hydrocarbon solvents as mentioned above.

The ground state geometries calculated for the H_2Pc/hydrocarbon clusters are shown in Fig. 5. The cluster binding energies and solute/solvent center-of-mass coordinates are listed in Table V. For $H_2Pc(C_2H_6)_1$, a geometry nearly isosenergetic with geometry II is calculated but not shown. The geometry is largely the same as II but has the C_2H_6 long axis rotated by 90° about the H_2Pc symmetry z axis with respect to geometry II. The geometry has a binding energy of 1564 cm^{-1}. For $H_2Pc(C_3H_8)_1$, two additional cluster geometries are calculated and not shown. Geometry III is similar to geometry II in that the solvent C_2 axis lies perpendicular to the H_2Pc molecular plane; however, the C_3H_8 is inverted in this geometry with respect to geometry I. The cluster binding energy is 1975 cm^{-1}. Geometry IV is nearly isoenergetic with geometry I. The geometry is largely the same as II but has the C_3H_8 rotated by 90° about the H_2Pc symmetry z axis. This geometry has a binding energy of 2202 cm^{-1}.

C. H_2O, MeOH, and EtOH clusters with H_2Pc and MgPc

Figures 6 and 7 and Table VI present the H_2O, MeOH, and EtOH solute solvent cluster spectra observed in the vicinity of their respective H_2Pc and MgPc 0_0^0 transitions. The H_2Pc cluster spectra are observed using $P_0 = 150$ psig helium, $T_e = 570$ °C, and $T_b = 435$ °C. The MgPc cluster spectra are observed using $P_0 = 135$ psig helium, $T_e = 630$ °C, and $T_b = 480$ °C.

The ground state geometries calculated for the above

TABLE V. Calculated cluster binding energies, solvent center-of-mass positions, and solvent orientation specifics.

Cluster	Fig. Ref.	Binding Energy (cm^{-1})	Location of solvent center-of-mass[a] x	y	z	Solvent orientation (remarks)
$H_2Pc(CH_4)_1$	5	1176	0.246	0.209	3.005	Three solvent hydrogens point toward solute
$H_2Pc(C_2H_6)_1$	5	1360	0.133	0.383	3.747	(I) Lower solvent CH_3 is situated as CH_4 in $H_2Pc(CH_4)_1$
	5	1574	0.672	0.022	3.206	(II) Centermost solvent CH_3 has two hydrogens toward solute
$H_2Pc(C_3H_8)_1$	5	2024	0.293	−0.929	3.456	(II) Terminal CH_3 groups on solvent point toward solute. Each CH_3 has two hydrogens pointing down
	5	2225	0.427	0.408	3.312	(I)
$H_2Pc(H_2O)_1$	8	1617	0.042	−0.030	2.550	Solvent hydrogens point toward solute
$H_2Pc(MeOH)_1$	8	1884	−0.101	0.260	2.985	Two solvent CH_3 hydrogens and hydroxyl hydrogens point toward solute
$H_2Pc(EtOH)_1$	8	2055	0.592	0.602	3.143	(I)
	8	2082	−0.013	−0.005	3.488	Solvent groups closest to solute are situated as MeOH in $H_2Pc(MeOH)_1$
$MgPc(H_2O)_1$	9	1553	0.492	1.478	3.011	Solvent hydrogens point toward solute
$MgPc(MeOH)_1$	9	2013	0.447	1.602	3.363	Solvent hydroxyl hydrogen points toward solute
$MgPc(EtOH)_1$	9	2954	−0.076	0.937	3.351	
$H_2Pc(CO_2)_1$	11	1992	0.126	0.017	2.784	
$Mg(CO_2)_1$	11	2336	0.986	1.937	3.142	

[a] The solute center-of-mass is located at $x = y = z = 0$ for all clusters.

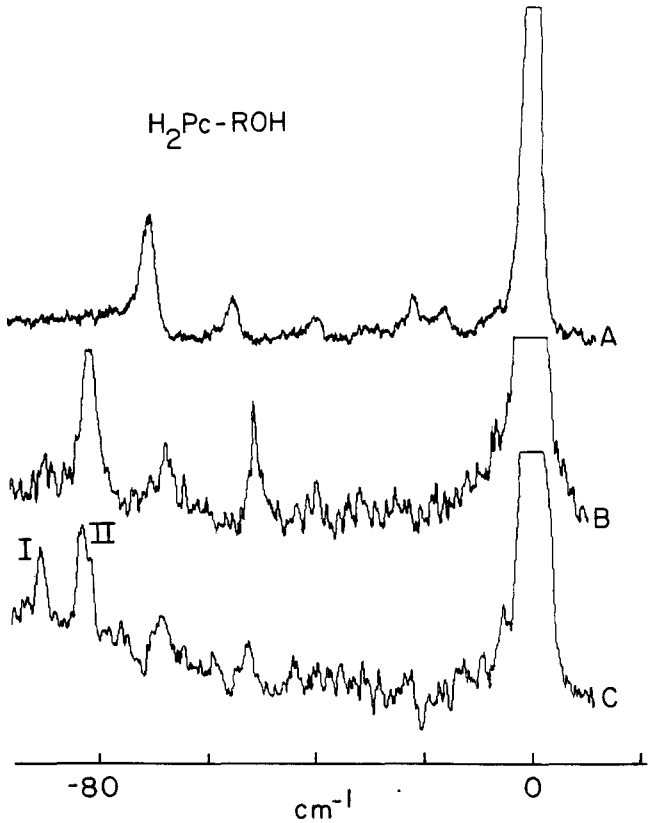

FIG. 6. FE spectra of H_2Pc/ROH clusters in the vicinity of the H_2Pc 0_0^0. The spectra are obtained using $T_e = 570$ °C, $T_b = 435$ °C, and $P_0 = 150$ psig He. Traces (A), (B), and (C) correspond to $H_2Pc(H_2O)_1$, $H_2Pc(MeOH)_1$, and $H_2Pc(EtOH)_1$, respectively. Peak assignments are given in Table VI.

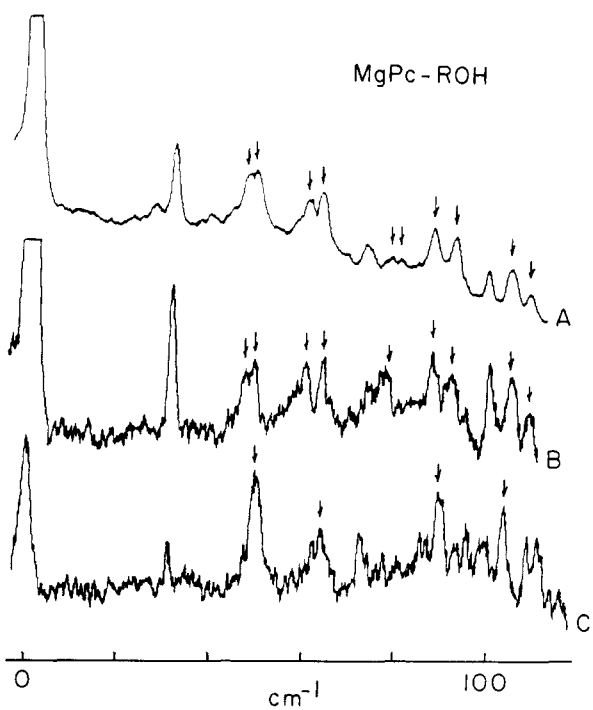

FIG. 7. FE spectra of MgPc/ROH clusters in the vicinity of the MgPc 0_0^0. Traces (A), (B), and (C) correspond to $MgPc(H_2O)_1$, $MgPc(MeOH)_1$, and $MgPc(EtOH)_1$, respectively. The spectra are taken at $T_e = 630$ °C, $T_b = 480$ °C, and $P_0 = 135$ psig He. Peak assignments are given in Table VI. The arrows indicate cluster transitons.

mentioned cluster series are shown in Figs. 8 and 9. The cluster binding energies and geometry specifics are listed in Table V. For $H_2Pc(EtOH)_1$, a geometry similar to geometry I is calculated but not shown. The cluster binding energy is 2053 cm^{-1}. This geometry has the EtOH rotated by 90° about the H_2Pc symmetry z axis with respect to I.

D. CO_2 clusters of H_2Pc and MgPc

The H_2Pc/CO_2 and $MgPc/CO_2$ FE spectra observed in the vicinity of the cluster chromophore 0_0^0 transitions are shown in Fig. 10. The cluster transition energies are listed in Table VII. In these experiments, both backing pressure and CO_2 concentration are varied. As in the H_2Pc/hydrocarbon cluster experiments, no new or additional sharp cluster transitions are observed under these conditions. The ground state cluster geometries for $H_2Pc(CO_2)_1$ and $MgPc(CO_2)_1$ are shown in Fig. 11. The cluster binding energies are listed in Table V.

IV. DISCUSSION

Before analyzing the individual cluster systems in detail, we will discuss the low frequency out-of-plane vibrational motion of isolated H_2Pc and MgPc. Elucidation of the out-of-plane motion in these molecules is essential to the understanding of the cluster spectra and in the identification of the number of different clusters of a specific composition observed. The nature of molecular motion associated with each spectral feature is determined by using the results of an out-of-plane normal coordinate analysis for isolated H_2Pc. Table I lists the nine lowest energy out-of-plane modes calculated. Given the qualitative nature of the force field used in the analysis, the calculated vibrational energies compare quite well with the fundamental energies inferred from the observed overtone transitions presented in Fig. 2 and Table II.

Three B_{1u} fundamentals are calculated at 14.8, 24.5, and 84.0 cm^{-1}. In the isolated H_2Pc spectrum, these vibrations are observed as symmetric overtones at 31.2 (A_0^2), 51.8 (B_0^2), 62.0 (A_0^4), and 163.7 (C_0^2) cm^{-1}. The symmetry forbidden fundamentals are thus located at 15.6, 25.9, and 81.9 cm^{-1} using a harmonic oscillator assumption. Two A_{1u} modes calculated at 33.1 and 71.7 cm^{-1} correspond to the forbidden out-of-plane fundamentals at 35.7 and 70.9 cm^{-1} which are observed as overtones at 71.4 (D_0^2), and 141.7 (E_0^2) cm^{-1}. The two B_{2g} (B_{3g}) modes calculated at 38.6 (38.2) and 72.1 (71.4) cm^{-1} correspond to the fundamentals of the observed overtone transitions at 85.4 and 100.6 (F_0^2 or H_0^2) cm^{-1} and at 176 and 203.1 (G_0^2 or J_0^2) cm^{-1}. The low energy out-of-plane vibronic transitions in the vicinity of the MgPc origin are similarly assigned (Fig. 3 and Table III).

Five out of the nine lowest energy out-of-plane vibrations are responsible for the vibronic transitions observed in the first 100 cm^{-1} the H_2Pc S_1 manifold. These five modes involve large amplitude displacements of the four isoindole groups comprising H_2Pc. The qualitative forms of the motion can be described by the two sets of operations indicated in Fig. 12: (a) the tilt of the isoindole groups around the line A through the pyrrole α carbons; and (b) the rotation of the

TABLE VI. $H_2Pc(H_2O)_1$, $H_2Pc(MeOH)_1$, $H_2Pc(EtOH)_1$, $MgPc(H_2O)_1$, $MgPc(MeOH)_1$, and $MgPc(EtOH)_1$ cluster transitions in the vicinities of the chromophore 0_0^0.

Species	Energy (vac. cm^{-1})	Cluster 0_0^0 relative to to $H_2Pc/MgPc$ 0_0^0 (cm^{-1})	Energy relative to cluster 0_0^0 (cm^{-1})	Assignment
$H_2Pc(H_2O)_1$	15 060.6	−71.2	0	0_0^0
	15 076.3		15.7	A_0^1
	15 091.8		31.2	A_0^2
	15 108.2		47.6	A_0^3
	15 115.7		55.1	B_0^2
$H_2Pc(MeOH)_1$	15 049.8	−82.0	0	0_0^0
	15 066.1		16.3	A_0^1
	15 081.2		31.4	A_0^2
$H_2Pc(EtOH)_1$	15 040.9	−90.9	0	$I\,0_0^0$
	15 035.3[a]		15.8	A_0^1
	15 051.7[a]		32.2	A_0^2
	15 048.5	−83.3	0	$II\,0_0^0$
	15 064.6		16.1	A_0^1
	15 080.2		31.7	A_0^2
$MgPc(H_2O)_1$	15 658.7	46.6	0	0_0^0
	15 672.6		13.9	A_0^1
	15 683.0			
	15 687.8		29.1	A_0^2
	15 696.4		37.7	F_0^1 or H_0^1
	15 715.8		57.1	B_0^2
	15 660.4	48.3	0	0_0^0
	15 674.5		14.2	A_0^1
	15 690.2		29.8	A_0^2
	15 701.0		40.6	F_0^1 or H_0^1
	15 717.3		56.9	B_0^2
$MgPc(MeOH)_1$	15 658.4	46.3	0	0_0^0
	15 672.5		14.1	A_0^1
	15 687.9		29.8	A_0^2
	15 696.8		38.4	F_0^1 or H_0^1
	15 713.7		55.3	B_0^2
	15 660.4	48.3	0	0_0^0
	15 674.8		14.4	A_0^1
	15 690.3		29.9	A_0^2
	15 701.2		40.8	F_0^1 or H_0^1
	15 717.8		57.4	B_0^2
$MgPc(EtOH)_1$	15 661.7	49.6	0	0_0^0
	15 676.3		14.6	A_0^1
	15 684.7			
	15 700.6		38.9	F_0^1 or H_0^1
	15 714.6		52.9	B_0^2

[a] Weak features (Fig. 6)—assignment must be considered tentative.

isoindole groups around the line B between the inner ring nitrogens and the midpoint between outer benzene carbons. The B_{1u} vibration calculated at 14.8 cm^{-1} corresponds to (a) type motion in which a set of opposite isoindole groups tilts out of the molecular plane in one direction and other set of opposite isoindole groups tilts out of the plane in the opposite direction. The B_{1u} vibration calculated at 24.5 cm^{-1} is similar to the 14.8 cm^{-1} mode; however, all the isoindole groups tilt out of the plane about the A axis (Fig. 12) in the same direction. The mode form looks similar to the forming of a "bowl" out of the phthalocyano skeleton. The A_u mode (33.1 cm^{-1}) involves type (b) motion of adjacent isoindole groups in one direction and the other two adjacent isoindole groups in the opposite direction. The motion looks like "ruffling" of the molecular skeleton. The B_{2g} mode (38.6 cm^{-1}) corresponds to (a) and (b) type motions of opposite isoin-

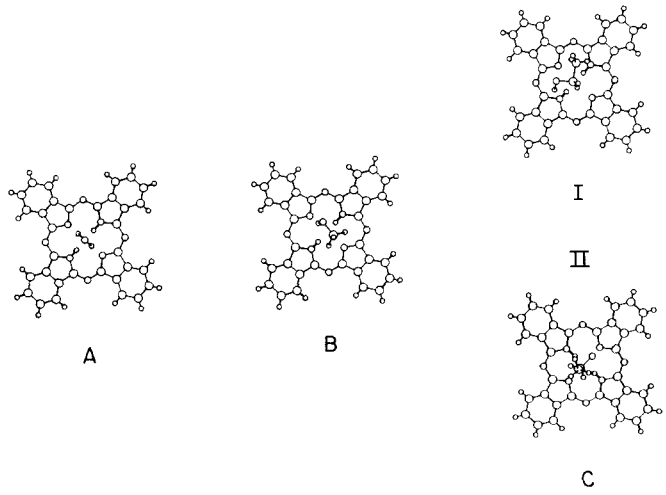

FIG. 8. Calculated minimum energy geometries for $H_2Pc(H_2O)_1$ (A), $H_2Pc(MeOH)_1$ (B), and $H_2Pc(EtOH)_1$ (C). The cluster binding energies and solute/solvent center-of-mass coordinates are given in Table V.

dole groups. The vibration form is such that one set of the opposite groups tilts out of the molecular plane about *A* in different directions. The other set of opposite groups rotates about *B* in the same direction. Overall, the motion looks similar to the forming of a "chair" out of the phthalocyano moiety. The B_{3g} mode (38.2 cm^{-1}) form is similar to that associated with the B_{2g} mode. The motion is the same in the both cases; however, the (a) and (b) motion is exchanged between the two opposite groups in the B_{3g} mode with respect to the motion in the B_{2g} mode.

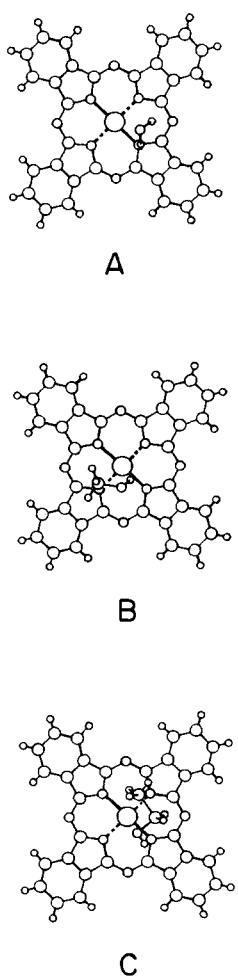

FIG. 9. Calculated minimum energy for $MgPc(H_2O)_1$ (A), $MgPc(MeOH)_1$ (B), and $MgPc(EtOH)_1$ (C). The cluster binding energies and solute/solvent center-of-mass coordinates are given in Table V.

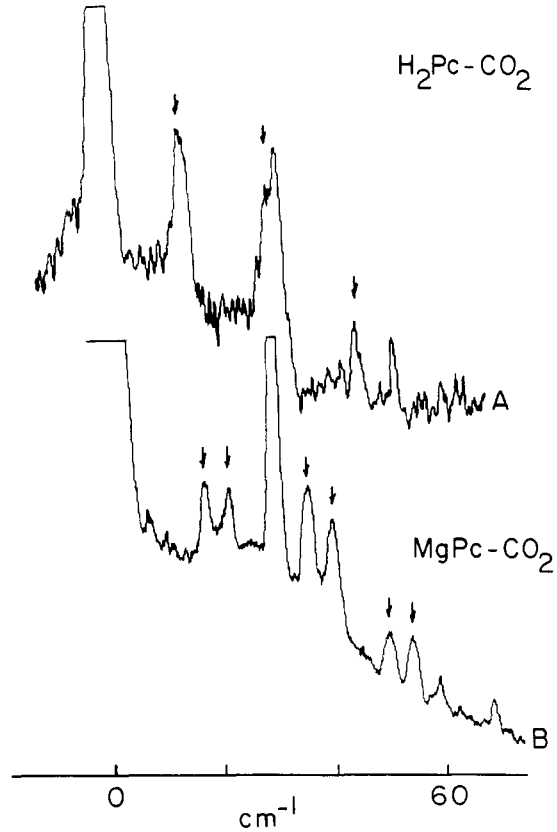

FIG. 10. FE spectra $H_2Pc(CO_2)_1$, and $MgPc(CO_2)_1$ in the vicinities of the cluster chromophore 0_0^0 transitions. The $H_2Pc(CO_2)_1$ spectrum (A) is taken at $T_e = 500$ °C, $T_b = 485$ °C, P_0 150 psig He, and 0.2% CO_2. The $MgPc(CO_2)_1$ spectrum (B) is taken at $T_e = 443$ °C, $T_b = 412$ °C, P_0 psig He, and 0.2% CO_2. Peak assignments are given in Table VII. The arrows indicate cluster transitions.

Chromophore out-of-plane fundamental and/or overtone transitions are observed in the vicinity of the cluster origins (*vide infra*) for all of the H_2Pc and MgPc systems discussed below. The observation of the cluster chromophore out-of-plane fundamentals in the cluster spectra can be rationalized using the results of the above normal coordinate analysis and group theoretical arguments: clusters have reduced symmetry with respect to the isolated chromophore H_2Pc or MgPc but nearly identical chromophore molecular vibrations. For example, in the $H_2Pc(H_2O)_1$, the symmetry is reduced from D_{2h} to, at most, C_{2v} (see Fig. 8). Under this reduced symmetry, the forbidden B_{1u} fundamental vibrations in isolated H_2Pc correlate to A_1 vibrations in C_{2v}. The modes are therefore fully allowed by symmetry and should, in principle, be observed if Frank–Condon factors are favorable.

vdW vibrational mode eigenvectors and eigenvalues have been calculated for a number of different solute/solvent

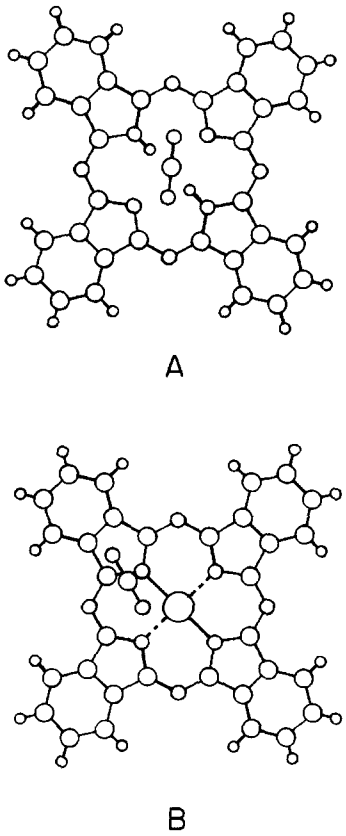

FIG. 11. Calculated minimum energy geometries for $H_2Pc(CO_2)_1$ (A) and $MgPc(CO_2)_1$ (B). The cluster binding energies and center-of-mass coordinates are given in Table V.

systems, including benzene, pyrazine, etc. with many of the same solvents employed in this work.[8] The calculated vdW mode energies compare quite well with those observed in the vibronic spectra for all the cluster systems analyzed. Based on the methods developed in these previous studies, we calculate that the lowest energy vdW modes for the H_2Pc and MgPc/solvent systems are ~ 50 cm^{-1}. Thus, features between cluster origins and $\sim +50$ cm^{-1} are most likely not vdW vibronic modes of the clusters. Moreover, these same studies demonstrate that high energy vdW modes (>50 cm^{-1}) do not have large intensity due to poor Franck–Condon factors. A fuller discussion of these issues is presented below.

On the basis of the above notions, the cluster spectra are analyzed using four premises. First, the cluster transitions are identified as those features not associated with the isolated H_2Pc or MgPc moiety. Second, the cluster origins are assigned to be the lowest energy cluster transitions observed. Third, the cluster vibronic manifolds associated with each of the origins should, and do, exhibit chromophore out-of-plane fundamental and overtone transitions (which have the same energy for all clusters) commensurate with those observed and/or calculated for isolated H_2Pc or MgPc. And fourth, due to the similarity between the vdW potential surfaces for the chromophore S_0 and S_1 states and the relatively large energies (see below) of the vdW modes in these systems, little if any vdW vibronic mode intensity should be observed. (Note that this expectation is also corroborated by porphyrin cluster spectra.[3(e),3(f)])

A. Hydrocarbon clusters of H_2Pc and MgPc

The H_2Pc/methane spectrum, Fig. 4(a) and Table IV, exhibits a cluster transition at 14.6 cm^{-1} to the red of the H_2Pc 0_0^0. This transition is assigned to the 0_0^0 of a single H_2Pc/methane species. As discussed above, features 31.3 and 51.3 cm^{-1} to the blue of the cluster 0_0^0 correspond to cluster chromophore out-of-plane symmetric overtones, A_0^2 and B_0^2. Both transitions are shifted by -14.6 cm^{-1} with respect to their corresponding transitions in the isolated H_2Pc spectrum. The A_0^1 transition is not observed as it may be weak and/or within the linewidth of the H_2Pc isolated molecule 0_0^0.

The cluster transitions are most likely due to $H_2Pc(CH_4)_1$ since no new additional sharp transitions are observed when either the CH_4 concentration or the backing pressure is increased. Increasing the CH_4 concentration and/or the backing pressure should yield higher order clusters. From prior experience with other solute/solvent cluster

TABLE VII. $H_2Pc(CO_2)_1$ and $MgPc(CO_2)_1$ cluster transitions in the vicinity of the chromophore 0_0^0.

Species	Energy (vac. cm^{-1})	Cluster 0_0^0 relative to H_2Pc/MgPc 0_0^0 (cm^{-1})	Energy relative to cluster 0_0^0 (cm^{-1})	Assignment
$H_2Pc(CO_2)_1$	15 145.8	14.0	0	0_0^0
	15 161.2		15.4	A_0^1
	15 176.5		30.7	A_0^2
$MgPc(CO_2)_1$	15 630.0	17.9[a]	0	0_0^0
	15 649.9		19.9	A_0^1
	15 664.6		34.6	A_0^2
	15 634.7	22.6[a]	0	0_0^0
	15 655.8		21.1	A_0^1
	15 667.0		32.3	A_0^2

[a] Transitions correspond to same cluster geometry species (see the text).

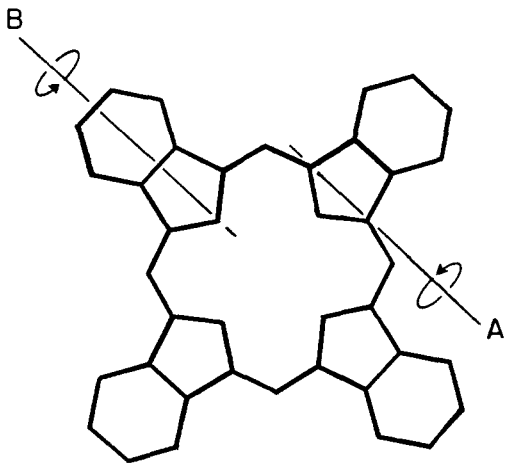

FIG. 12. Operations showing qualitative out-of-plane vibrational motion in $H_2Pc/MgPc$.

systems,[1(f),1(g),6] higher order clusters typically yield more than one set of cluster transitions. Additive shifts are also observed in most cases resulting from inhomogeneous nucleation processes in which solvent molecules bind symmetrically to opposite sides of the chromophore molecular plane.

The predominance of 1:1 solute/solvent clusters in the expansion may be rationalized on the basis of large solute/solvent binding energy vs small solvent dimer binding energy.[6] In the systems presently studied, the solute/solvent binding energies are sufficiently large that when a solvent dimer collides with a solute molecule, the dimer dissipates some of the cluster binding energy via vibrational predissociation. This interactive collision leaves one solvent molecule bound to the solute while the other solvent carries off enough of the cluster energy to stabilize the vdW bond until further collisional cooling can take place. These notions would lead one to conclude that 1:1 solute/solvent clustering predominates in the other clusters systems analyzed as well. Apparently this cluster nucleation and growth mechanism is quite general for many different clusters.[6]

The existence of a single $H_2Pc(CH_4)_1$ geometry responsible for the cluster origin in the spectrum is further corroborated by the ground state configuration calculation depicted in Fig. 5(a). In this geometry, the CH_4 cluster subunit is situated above the H_2Pc plane and is coordinated to the π-cloud of the aromatic ring. The cluster geometry is interesting in the respect that the cluster solvent uniquely lies nearly over the H_2Pc core: none of the several potential solvation sites located over each of the H_2Pc closed ring subunits is apparently a true local potential energy minimum. One can envision three distinct cluster sites on the H_2Pc moiety: (1) above the H_2Pc core (most stable); (2) above one of its four five-membered rings; or (3) above one of its four six-membered rings (least stable). If all three of these sites were physically accessible, three different cluster spectral shifts should be observed corresponding to the three distinct sites. Since the single cluster origin in the spectrum suggests that only one geometry is stable, two out of the three speculated minima are either nonexistent or not sufficiently deep to accommodate bound state geometries. The observed cluster origin at $-14.6\ cm^{-1}$ from the $H_2Pc\ 0_0^0$ probably corresponds to a geometry very similar to the calculated one [Fig. 5(a)].

H_2Pc clustered with ethane, Fig. 4(b) and Table IV, reveals two cluster origins at 25.9 and 18.8 cm^{-1} to the red of the $H_2Pc\ 0_0^0$. Two weak transitions to the blue of the $H_2Pc\ 0_0^0$ correspond to cluster chromophore out-of-plane vibrations A_0^2 built upon the two cluster origins. The transition at $-10.3\ cm^{-1}$ corresponds to the fundamental of the out-of-plane cluster chromophore vibration A_0^1 ($15.6\ cm^{-1}$) built upon the origin at $-25.9\ cm^{-1}$. The cluster chromophore fundamental built upon the cluster origin at $-18.8\ cm^{-1}$ is not observed as it may be weak and/or within the linewidth of the $H_2Pc\ 0_0^0$.

These cluster manifolds most likely correspond to $H_2Pc(C_2H_6)_1$ clusters since, as in the $H_2Pc(CH_4)_1$ case, as both concentration and backing pressure are varied, the spectrum does not yield any additional sharp transitions. Furthermore, no additive spectral shifts are observed indicative of higher order clusters with ethane subunits situated above and below the H_2Pc plane. The same arguments used to rationalize the predominance of 1:1 clusters in the $H_2Pc(CH_4)_1$ case are applicable to this system as well.

The two $H_2Pc(C_2H_6)_1$ cluster geometries shown in Fig. 5(b) support the assignment of two cluster geometries. Both geometries have the C_2H_6 situated over the center of the H_2Pc core as found for $H_2Pc(CH_4)_1$. Geometry I should yield a larger spectral shift than geometry II based upon polarizability arguments previously discussed for single ring cluster systems.[1(g),20] Briefly, the species with the larger spectral shift is associated with the solute/solvent relative orientation for which the direction of the large solvent polarizability is perpendicular to the solute molecular plane. Using this argument, a geometry similar to I would be associated with the cluster origin 25.9 cm^{-1} to the red of the $H_2Pc\ 0_0^0$. As mentioned in the Results section, two specific solvent orientations are consistent with the qualitative solute/solvent geometry of calculated $H_2Pc(C_2H_6)_1$ configuration II [see Fig. 5(b)]. One would not expect a spectroscopic difference between the two geometries as they differ by a 90° rotation about the symmetry z axis of H_2Pc. These two directions as far as the H_2Pc moiety is concerned should be roughly equivalent in terms of polarizabilities and π-cloud overlap.

The H_2Pc/propane clusters, Fig. 4(c) and Table IV, are assigned on the basis of similar arguments presented for the other two hydrocarbon clusters studied. In the spectrum, two $H_2Pc(C_3H_8)_1$ cluster origins appear at 33.4 and 25.1 cm^{-1} to the red of the $H_2Pc\ 0_0^0$. Two cluster vibronic manifolds to the blue of each origin are assigned to cluster chromophore vibronic fundamentals and first overtones. For the cluster manifold beginning at $-33.4\ cm^{-1}$, the A_0^1 occurs at 14.8 cm^{-1} to the blue of the cluster 0_0^0. For the cluster manifold beginning at $-25.1\ cm^{-1}$, the A_0^1 and A_0^2 occur at 15.7 and 31.4 cm^{-1} to the blue of the cluster 0_0^0.

Geometries similar to those shown in Fig. 5(c) could be associated with the two observed cluster manifolds. Differ-

ent spectral shifts for the two geometries most likely result from difference in π-cloud solvation. The propane solvent interacts less with the H_2Pc π cloud in geometry II than in geometry I since the C_2 axis of the cluster solvent (direction of small polarizability) is perpendicular to the H_2Pc molecular plane in geometry II but parallel to the plane in geometry I. A geometry similar to I could thus be responsible for the cluster manifold beginning at $-33.4\ cm^{-1}$ and a geometry similar to II could be associated with the manifold beginning at $-25.1\ cm^{-1}$.

The $H_2Pc(C_2H_6)_1$ and the $H_2Pc(C_3H_8)_1$ spectra exhibit A_0^1 transitions which are forbidden in isolated H_2Pc. A similar change in selection rules upon clustering has been reported for the benzene/solvent systems.[1(f),1(g),8] In the latter systems, the observations suggest that the presence of the cluster solvent over the solute molecular plane is sufficient to induce the forbidden benzene 0_0^0 transition if the threefold rotation axis of the solute is destroyed. Furthermore, the selection rules governing the intermolecular vdW motion follow the reduced symmetry of the cluster systems. This minimum perturbation may also be the driving force which induces the vibronic transitions in the H_2Pc/hydrocarbon clusters. The perturbation in the present instance may even be large enough to cause the cluster chromophore to adjust its geometry to establish optimal π-cloud overlap. The observation of the B_{1u} fundamental at $15\ cm^{-1}$ serves as evidence supporting this notion as molecular displacement along this coordinate appears to yield favorable Franck–Condon factors. The A_0^1 transition is also observed in all the other H_2Pc and MgPc clusters studied as well. These observations would lead one to conclude that the H_2Pc and MgPc molecules in the clusters are not planar in the excited electronic state. In spite of this change in *molecular* out-of-plane potential for H_2Pc (and MgPc), the overall vdW potentials for the ground and excited states still remain quite similar as no *intermolecular cluster* vdW modes are identified in the various cluster spectra.

The one major difference between the H_2Pc/hydrocarbon cluster spectra and the benzene/hdyrocarbon cluster spectra is the absence of observable intermolecular vdW mode intensity in the H_2Pc cluster spectra. The lowest energy vdW motion (bending) is expected to be observed at about $50\ cm^{-1}$ to the blue of the cluster origins based upon calculational modeling of intermolecular mode energetics.[8] The vdW stretch is expected to occur at about $100\ cm^{-1}$ above the cluster origin. The absence of $\Delta v = \pm 1$ vdW mode transitions in the H_2Pc clusters may be due to poor Franck–Condon factors. The large size and extensive delocalization of the H_2Pc π cloud yields little change in the electron density at the cluster site when a single electron is promoted from a π to a π^* orbital. Thus, one might expect that the intermolecular potential surfaces of the two states are nearly superimposable even though the binding energy of the excited state is slightly different ($\sim 1\%$) than that of the ground state. The net result is the observation of vdW sequence structure ($\Delta v = 0$) giving rise to cluster origins and cluster chromophore vibrations only. These arguments probably hold for all the cluster systems investigated in this study as well.

B. H_2O, MeOH, and EtOH clusters of H_2Pc and MgPc

H_2Pc clustered with H_2O, Fig. 6(a) and Table VI, yields a spectrum exhibiting a single cluster vibronic manifold with an origin $71.2\ cm^{-1}$ to the red of the H_2Pc 0_0^0. The single cluster (chromophore) vibronic manifold suggests that one H_2Pc/H_2O species is responsible for the observed spectrum. The spectrum is assigned to $H_2Pc(H_2O)_1$ based upon the same arguments developed for the H_2Pc/hydrocarbon clusters. The assignment is supported by the ground state configuration calculations for which a single geometry is obtained, Fig. 8(a). In this geometry, the H_2O is situated over the H_2Pc core. The transitions at 15.7, 31.2, and $47.6\ cm^{-1}$ to the blue of the cluster 0_0^0 correspond to H_2Pc out-of-plane vibrations A_0^1, A_0^2, and A_0^3. The feature at $55.1\ cm^{-1}$ to the blue of the cluster 0_0^0 corresponds to the B_0^2 cluster chromophore transition.

Clustering H_2Pc with MeOH yields a cluster spectrum, Fig. 6(b) and Table VI, associated with $H_2Pc(MeOH)_1$ which has an origin $82.0\ cm^{-1}$ to the red of the H_2Pc 0_0^0. The cluster chromophore out-of-plane vibrations A_0^1 and A_0^2 are observed at 16.3 and $31.4\ cm^{-1}$ to the blue of the cluster 0_0^0. The assignment of a single cluster manifold is supported by the single calculated ground state geometry obtained [Fig. 8(b)].

H_2Pc cluster with EtOH, Fig. 6(c) and Table VI, yields a spectrum exhibiting two cluster (chromophore) vibronic manifolds which can be assigned as due to two $H_2Pc(EtOH)_1$ species. The first cluster origin is at $90.9\ cm^{-1}$ to the red of the H_2Pc 0_0^0 and the second cluster manifold begins at $83.3\ cm^{-1}$ to the red of the H_2Pc 0_0^0. The cluster chromophore vibrations A_0^1 and A_0^2 can be identified in these manifolds at 16.1 and $31.7\ cm^{-1}$.

The two $H_2Pc(EtOH)_1$ cluster species responsible for the observed spectrum can be associated with geometries similar to those shown in Fig. 8(c). In geometry I the EtOH solvent interacts more with the H_2Pc π cloud than in geometry II and, therefore, geometry I should exhibit a larger spectral shift. Thus a geometry similar to I could be associated with the cluster whose origin is at $-90.9\ cm^{-1}$ and a geometry similar to II could be associated with the cluster whose origin is at $-83.3\ cm^{-1}$ with respect to the H_2Pc 0_0^0.

The H_2Pc/H_2O, /MeOH, and /EtOH cluster spectra suggest that the solvent OH group is intimately involved in the intermolecular interaction. The red shifts for all three clusters are similar and larger than those observed in the H_2Pc/hydrocarbon systems. The MeOH and EtOH cluster shifts are larger than that observed in the H_2O cluster suggesting that the shifts are dependent upon the combined effects of the OH group and the hydrophobic portions of the cluster solvents. If, on the other hand, the alkyl groups were pointing toward the solute, one would expect the spectral shifts for MeOH/EtOH clusters to be similar to those observed in the hydrocarbon clusters. In these geometries, the alkyl groups would be the major contributors in the intermolecular interaction.

The large spectral shifts, the interaction of the OH group with H_2Pc and the ground state configuration calculations lead one to postulate that hydrogen bonding may be

occurring in these cluster systems. Hydrogen bonding can occur to some extent between the solute inner ring nitrogens and/or pyrrole hydrogens and the solvent OH group: the H_2Pc inner ring nitrogens have large electron density[5,21] which can enhance the hydrogen bonding of solvent OH groups. Since the observed chromophore transition is $\pi^* \leftarrow \pi$, a large red shift can be expected.

The $MgPc(H_2O)_1$, $(MeOH)_1$, $(EtOH)_1$ cluster spectra, Fig. 7 and Table VI, are very similar to one another. The $MgPc(H_2O)_1$ spectrum can be assigned as arising from two different cluster manifolds with origins at 46.6 and 48.3 cm^{-1} to the blue of the MgPc 0_0^0. Cluster chromophore out-of-plane vibrations are observed for both manifolds. The A_0^1 and the A_0^2 are observed at 13.9 (14.2) and 29.1 (29.8) cm^{-1} to the blue of the origins. B_0^2 transitions are observed at 57.1 (56.9) cm^{-1}. The $MgPc(MeOH)_1$ and $MgPc(EtOH)_1$ spectra are similarly assigned.

The $MgPc(ROH)_1$ series differs from the $H_2Pc(ROH)_1$ series in three aspects. First, the $MgPc(ROH)_1$ spectra exhibit hypsochromic shifts with respect to the isolated MgPc spectrum. The direction of the spectral shifts indicate that the solute and solvents interact more strongly in S_0 than in S_1. The major difference between the two solute systems studied is the phthalocyano core environment: the pyrrole hydrogens in H_2Pc are replaced by a magnesium in MgPc. The hypsochromic shift suggests that the core is responsible for the larger ground state interaction. The greater stabilization in the ground state can, in principle, be due to interactions ranging from weak nonbonded vdW interactions to actual complexation in which the solvent donates an electron pair to the solute via the central metal atom.[5] On the basis of the size of the spectral shifts observed, the interaction is most likely due to weak vdW interactions. If the solvent were to donate significant electron density to the central Mg atom in MgPc (a coordination bond formation) or if the Mg were to move significantly out of the Pc molecular plane,[22] cluster formation would drastically perturb the chromophore electronic environment and yield relatively large spectral shifts. Observation of weak vdW interactions between MgPc and H_2O, EtOH, and phenol in the IR region leads to similar conclusions.[23]

Second, the spectral shifts in the $MgPc(ROH)_1$ series are virtually identical. This observation suggests that the OH group is intimately involved in the interaction and, furthermore, is largely responsible for the observed spectral shifts. The ground state configuration calculations, Fig. 9, support the notion that the OH group is the major contributor to the interaction. All three calculated geometries depicted in Fig. 9 have the solvents situated so that the OH groups point towards the MgPc core. Moreover, one would not expect to observe sharp cluster transitions if the hydrophobic portions of the solvents were the major contributors to the interaction.

Third, the $MgPc(ROH)_1$ spectra show two nearly isoenergetic cluster origins and vibronic manifolds. These cluster features could be due to either two cluster species which are nearly spectroscopically identical or they could be due to the splitting of the twofold degenerate chromophore S_1 state via vdW cluster formation. The former situation probably does not occur since these doublets are present in all the MgPc clusters observed. One would not typically expect to see this type of coincidence in the different cluster systems especially when two solvent series are considered. In MgPc clusters, clustering reduces the system symmetry (see Fig. 9, for example) and the fourfold symmetry axis of the MgPc chromophore is destroyed. The degenerate Q band (E_u in D_{4h}) may thus split into Q_x and Q_y bands (B_{2u} and B_{3u} in D_{2h}); the splitting is small, however, due to the small perturbation caused by vdW clustering. Similar removal of degeneracies occurs for benzene clusters[1(g),8,20] and for ground state vibrations of MgPc/H_2O, /EtOH, and /phenol systems.[23]

C. CO_2 clusters of H_2Pc and MgPc

H_2Pc clustered with CO_2, Fig. 10(a) and Table VII, yields a spectrum with a single cluster origin blue shifted by 14 cm^{-1} with respect to the isolated H_2Pc 0_0^0. The cluster manifold is assigned to a $H_2Pc(CO_2)_1$ species. Cluster chromophore out-of-plane vibrations A_0^1 (15.4 cm^{-1}) and A_0^2 (30.7 cm^{-1}) built upon the cluster origin are also observed. The calculated ground state geometry, Fig. 11(a), further supports the existence of a single cluster species responsible for the spectrum. In this geometry, the CO_2 moiety is situated over the H_2Pc core.

The $H_2Pc(CO_2)_1$ spectrum is different than the other H_2Pc clusters studied in that it is the only system exhibiting a hypsochromic shift. The exact nature of the interaction responsible for the spectral shift in this system is not known and more work on CO_2 solute/solvent systems is necessary to establish a firm argument.[6(c)] On the basis of the interactions responsible for the spectral shifts in the hydrocarbon and hydrogen bonded solute/solvent systems, the major interaction responsible for the shift appears to involve solvent/solute π-cloud overlap. In the ground state, the solute and solvent most likely interact through π–π interactions. Upon excitation the diffuse nature of the solute π^* state reduces the interaction between the π systems and results in a loss in S_1 binding energy relative to S_0.

MgPc clustered with CO_2, Fig. 10(b) and Table VII, reveals a cluster spectrum with two parallel vibronic progressions. The appearance of the two cluster manifolds is probably due to the same type of electronic state splitting that occurs in the $MgPc(ROH)_1$ systems. The cluster origins are blue shifted by 17.9 and 22.6 cm^{-1} with respect to the MgPc 0_0^0. As in $H_2Pc(CO_2)_1$ well defined cluster chromophore vibronic transitions are observed. The A_0^1 and A_0^2 transitions built upon the origin at 17.9 cm^{-1} occur at 19.9 and 31.1 cm^{-1} to the blue of this origin. The A_0^1 and A_0^2 transitions built upon the 22.6 cm^{-1} origin occur at 21.1 and 32.3 cm^{-1} to the blue of the origin. The existence of a single $MgPc(CO_2)_1$ species responsible for the cluster transitions is supported by the ground state configuration calculation shown in Fig. 11(b).

The $MgPc(CO_2)_1$ cluster spectrum differs from that of the other MgPc clusters studied in that the magnitude of the hypsochromic shift is smaller for $MgPc(CO_2)_1$. This difference can possibly be attributed to the difference in the major mode of interaction between the solute and solvent. In

$MgPc(CO_2)_1$, the major interaction may be due to the same type of π-cloud interaction as suggested for the $H_2Pc(CO_2)_1$ interaction as the spectral shifts are comparable for the two systems. If the solvent oxygen/solute magnesium interaction were the major contributor, one could expect a larger hypsochromic shift comparable to those found for the $MgPc(ROH)_1$ systems.

Previous studies of clusters of Zn porphyrin with benzene, methanol, water, acetonitrile, and pyridine[3e] consistently evidence much larger ($\gtrsim 100\ cm^{-1}$) red shifts than those reported herein. These large shifts for the Zn porphyrins must be associated either with the porphyrin or the Zn entity; perhaps the central Zn atom interacts strongly with these solvents. Studies of the free base porphine $(Ar)_1$ cluster have also been reported[3f]: spectroscopic shifts for this system also appear to be larger than those reported here for H_2Pc. A possible source of this increased shift for porphyrin systems over phthalocyano systems may be increased π-electron density over the central portion of the porphyrin macrocycle ring compared to the Pc macrocycle ring.

V. SUMMARY AND CONCLUSIONS

FE spectroscopy is used to probe the optical spectra of vdW clusters of H_2Pc and MgPc in the vicinity of the cluster 0_0^0 transitions. A continuous supersonic molecular jet capable of operating at temperatures up to 650 °C is employed to generate the ultracold molecular beam. Spectroscopic observables, such as spectral shift and forbidden chromophore vibronic transitions, combined with computer modeling of ground state cluster intermolecular interactions, allow for the elucidation of the nature of the intermolecular potential and qualitative geometry of the H_2Pc and MgPc clusters studied. The conclusions drawn for this work are as follows:

(1) The cluster vibronic spectra and theoretical calculations suggest that stable H_2Pc and MgPc clusters have solvents situated over the center of the phthalocyano core. Local minima over peripheral solute rings are either nonexistent or too shallow to accommodate minimum energy bound state geometries.

(2) H_2Pc/hydrocarbon clusters are similar to the benzene and *N*-heterocycle/hydrocarbon clusters previously studied. The spectral shifts in these solute/solvent series are all bathychromic. The magnitudes of the spectral shifts increase with increasing solvent size and polarizability. The qualitative cluster geometries responsible for the observed spectra are similar with respect to solute/solvent orientation is concerned.

(3) In both H_2Pc and MgPc clusters, the H_2O, MeOH, and EtOH moieties are situated over the Pc core in such a manner that the OH groups are intimately involved in the intermolecular interactions and contribute significantly to the spectral shifts.

(4) Hydrogen bonding may be occurring to some extent between H_2Pc and solvent ROH moieties.

(5) MgPc clusters display weak vdW interactions between the cluster solute and solvent. Actual complexation in which the solvent donates an electron pair to the solute does not occur

(6) Forbidden low frequency cluster chromophore out-of-plane vibronic transitions are induced by clustering in both H_2Pc and MgPc systems. Intensity due to this motion arises from the reduction of the chromophore symmetry in the clusters. The perturbation may be large enough to cause the cluster chromophore geometry to change in an attempt to maximize π-cloud overlap with the solvent.

(7) Excited electronic state splitting occurs in the MgPc clusters due to the reduction in system symmetry upon cluster formation. The degenerate Q band appears to split into its two components, Q_x and Q_y.

[1](a) D. H. Levy, L. Wharton, and R. E. Smalley, *Chemical and Biochemical Applications of Lasers* (Academic, New York, 1977), Vol. II; (b) T. D. Mark and A. W. Castleman, Jr., Adv. At. Mol. Phys. **20**, 65 (1985); (c) A. Amirav, U. Even, and J. Jortner, J. Chem. Phys. **75**, 2489 (1981); (d) T. R. Hays, W. Henke, H. L. Selzle, and E. W. Schlag, Chem. Phys. Lett. **77**, 19 (1981); (e) P. M. Felker and A. H. Zewail, *ibid.* **94**, 454 (1983); (f) J. Wanna, J. A. Menapace, and E. R. Bernstein, J. Chem. Phys. **85**, 1795 (1986); (g) M. Schauer and E. R. Bernstein, *ibid.* **82**, 726 (1985).

[2](a) P. S. H. Fitch, C. A. Haynam, and D. H. Levy, J. Chem. Phys. **73**, 1064 (1980); (b)**74**, 6612 (1981); (c) **70**, 2018 (1979).

[3](a) U. Even, J. Magen, and J.Jortner, J. Chem. Phys. **77**, 4374 (1982); (b) **77**, 4384 (1982); (c) **76**, 5684 (1982); (d) U. Even and J. Jortner, *ibid.* **77**, 4391 (1982); (e) J. Phys. Chem. **87**, 28 (1983); (f) U. Even, J. Jortner, and Z. Berkovitch-Yellin, Can. J. Chem. **63**, 2073 (1985).

[4]J. Barber, *Primary Processes of Photosynthesis* (Elsevier, New York, 1977).

[5]D. Dolphin, *The Porphyrins* (Academic, New York, 1979), Vols. III, V, and VII; J. E. Falk, *Porphyrins and Metalloporphyrins* (Elsevier, New York, 1964).

[6](a) E. R. Bernstein, K. Law, and M. Schauer, J. Chem. Phys. **80**, 207 (1984); (b) M. Schauer, K. S. Law, and E. R. Bernstein, *ibid.* **82**, 736 (1985); (c) R. Nowak and E. R. Bernstein, *ibid.* (to be published).

[7](a) F. A. Momany, L. M. Carruthers, R. F. McGuire, and H. A. Scheraga, J. Phys. Chem. **78**, 1595 (1974); (b) G. Nemethy, M. S. Pottle, and H. A. Scheraga, *ibid.* **87**, 1883 (1983).

[8]J. A. Menapace and E. R. Bernstein, J. Phys. Chem. **91**, 2533, 2843 (1987).

[9]B. F. Hoskins and S. A. Mason, Chem. Commun. **1969**, 554. The phthalocyano skeleton in MgPc is assumed to be the same as H_2Pc in the calculations. The H_2Pc imino hydrogens are replaced by a magnesium atom at the centermost position to model the MgPc structure.

[10]T. M. Miller and B. Bederson, Adv. At. Mol. Phys. **13**, 1 (1977).

[11]A. Bondi, J. Phys. Chem. **68**, 441 (1964).

[12]R. A. Scott and H. A.Scheraga, J. Chem. Phys. **45**, 2091 (1965).

[13](a) A. Henriksson and M. Sundbom, Theor. Chim. Acta. (Berl.) **27**, 213 (1972); (b) A. M. Schaffer, M. Gouterman, and E. R. Davidson, *ibid.* **30**, 9 (1973).

[14]G. Herzberg, *Molecular Spectra and Molecular Structure III. Electronic Spectra and Electronic Structure of Polyatomic Molecules* (van Nostrand, New York, 1966).

[15]R. F. McGuire, F. A. Momany, and H. A. Scheraga, J. Phys. Chem. **76**, 375 (1972).

[16]P. Jönsson, Acta Crystallogr. Sect. B **32** 232 (1976).

[17]E. B. Wilson, Jr., J. C. Decius, and P. C. Cross, *Molecular Vibrations: Theory of Infrared and Raman Vibrational Spectra* (McGraw–Hill, New York, 1955).

[18]J. A. Menapace, Ph.D. thesis, Colorado State University, 1987.

[19]P. C. Painter and J. L. Koenig, Spectrochim. Acta Part A **33**, 1019 (1977).

[20]J. Wanna and E. R. Bernstein, J. Chem. Phys. **84**, 927 (1986).

[21]H. C. Longuet-Higgins, C. W. Rector, and J. R. Platt, J. Chem. Phys. **18**, 1174 (1950).

[22]M. S. Fischer, D. H. Templeton, A. Zalkin, and M. Calvin, J. Am. Chem. Soc. **93**, 2622 (1971).

[23]B. Stymne, F. X. Sauvage, and G. Wettermark, Spectrochim. Acta Part A **35**, 1195 (1979).